DEGREE PROJECT IN AEROSPACE ENGINEERING,
SECOND CYCLE, 30 CREDITS
STOCKHOLM, *SWEDEN 2020*

Optical Payload Mounting Interface Design for a Quantum Key Distribution CubeSat Telescope In-Orbit Demonstration

LUKAS JAKAS

KTH ROYAL INSTITUTE OF TECHNOLOGY
SCHOOL OF ENGINEERING SCIENCES

Abstract

Although free-space optical communication systems require to overcome demanding precision requirements for their optical payload, the photonics company mBryonics has taken on the challenge of designing a quantum key distribution telescope for an in-orbit demonstration mission on a CubeSat platform. A part of the task was formulated as a thesis project which is reported in this document. The approach was to first complete a comprehensive literature review, then compile a system requirement review document, carry out trade studies for different telescope components and, finally, run numerous finite element analysis studies which let to come up with an optimal system configuration. The project outcome was satisfactory – the optical payload structure was designed to be robust enough to endure harsh rocket launch and space environment while at the same time decoupling the essential telescope elements from temperature fluctuations and vibrations.

Sammanfattning

Optisk kommunikation via satelliter i omloppsbana ställer höga krav på precisionen i den optiska nyttolasten. Fotonikföretaget mBryonics har antagit utmaningen att utveckla ett teleskop som använder kvantnyckelfördelning och avser demonstrera detta på en CubeSat-plattform. En del av utvecklingen formulerades som ett examensarbete som presenteras i denna rapport. Arbetet omfattar en omfattande litteraturstudie, framtagande av ett krav/verifieringsdokument, en genomlysning av olika teleskopkomponenter och slutligen ett antal simuleringar med finita element analys för att finna en fullgod systemlösning. Projektresultatet var tillfredsställande – det optiska systemet bekräftades vara tillräckligt robust för att klara av de extrema belastningar som uppkommer under uppskjutning och i dess slutliga omloppsbana, genom att isolera kritiska teleskopkomponenter från termiska laster och vibrationer.

Preface

This thesis is the final work of my master's studies at the KTH Royal Institute of Technology. It presents the results of the preliminary design of a novel type of space optical device. This was a fascinating project to work on as it had a real purpose in an industry I am so passionate about.

What has become a true learning experience would not be possible without the mBryonics team giving me trust in this challenging task. Special thanks go to David for his patience when answering my countless questions and sharing his valuable advice.

I would also like to forward gratitude to my parents for the support throughout the pursuit of my postgraduate degree.

Table of Contents

1. Introduction

Free-space optical communication (FSO) is the technology of data transmission in space of the future. It uses lasers to provide optical bandwidth connections in air or vacuum. Comparing to the old-fashioned radio frequency (RF) technology, optical communication systems use wavelengths that are shorter by several magnitudes. This offers several significant advantages including large bandwidth modulation and high data rates. What is more, FSO has low diffraction losses and the possibility to build more efficient hardware when compared to RF systems. All of this means the potential to meet low size, weight and power requirements that are all popular spacecraft system qualities during the "New Space" age. Several in-orbit demonstrations (IOD's) of FSO were already performed, even for missions that extended beyond the Earth's orbit. However, to become used more widely in the industry, the cost of the technology should be reduced [1].

FSO is also the technology that an Ireland-based photonics company called mBryonics is building its quantum key distribution (QKD) CubeSat telescope on. It is set to be launched for an IOD mission on a 6U CubeSat in 2022. Critical to mission's success is the opto-mechanical design, which requires some careful engineering to meet the high precision requirements of a typical optical system design. Even with considerate optical design the alignment of most optical payloads needs to be maintained to a micron level precision over a wide range of operating temperatures. Additionally, the spacecraft is at mercy of a harsh vibrational environment during the space launch. This requires a clever design of the optical payload mounts and interfaces to the satellite bus that decouple the satellite structure deformations from the optical system.

To come up with a preliminary design of such structure is exactly what the objective of this thesis project is. The main engineering work will be focused on a monolithic flexure design that primary and secondary mirrors of the telescope will be mounted on. The structure design should minimise optical distortions and optimise telescope's performance in the operational environment. However, in order to successfully develop it, the project scope extends beyond that. Firstly, a preliminary literature review will be performed. It will include the research on mentioned technology, as well as the standards and requirements used throughout the industry. After these are identified, a system requirements review (SRR) will be compiled. The SRR will highlight the key telescope mechanical requirements and will contain the first iteration of the telescope's test plan. Following the successful SRR, the preliminary design of the optical payload mounting structure will be devised. The mechanical performance predictions of the optical system will rely heavily on finite element analysis (FEA). Therefore, numerous different simulations will be done on the telescope's model using the Autodesk Fusion 360 CAD software. Numbers obtained from analysis will be compared with design restrictions defined in the SRR and by the company's optical engineers.

The project is to an extent classified by mBryonics. This means that certain points of its outcome will not be revealed in this report. In particular, the exact optical payload dimensions, the looks of the inside of the telescope, component design details, mirror coating materials and some FEA simulation result specifics will be omitted.

2. Background

2.1 Decoupling Mounts

Flexures are mechanical devices used to decouple optical elements from mechanical and thermal effects so that they are minimized and the impact on the optical instrument performance is mitigated. The ideal flexure mount is a kinematic mount which supports three orthogonal axes at three infinitesimal points. In reality, such contact would introduce very high stresses which would limit the use of kinematic design to small and lightweight components [2]. Instead, a semi-kinematic model with a finite contact area is adopted and a monolithic flexure can be regarded as one. The location of a flexure is determined by kinematic principle which says that the line of support forces must pass through the centre of gravity (CoG) of an optical component. In other words, radial compliance is the way to make an optical system athermal while maintaining its alignment [3].

A bipod flexure is the most common support type for high-precision mirror mount applications. Its construction is equivalent to a cross-strip flexure. Usually, three bipods are attached to the mirror back or edge. Their construction and configuration can be seen in figure 2.1.

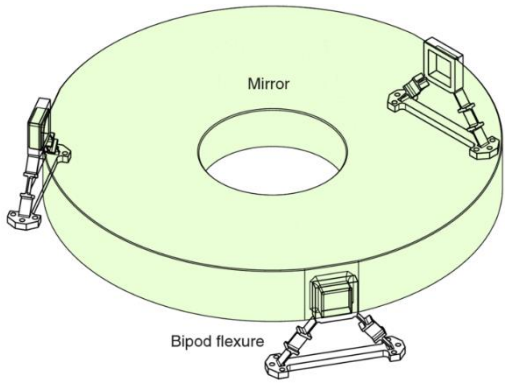

Figure 2.1 An example of a bipod support for a mirror.

Such a system offers the convenience of changing the angle between the two flexures of a bipod which in turn adjusts the centre of the pivot motion. It is also good for isolation from both vibrational and thermal environment changes. On the other hand, bipods require additional space below or on the side of an optical element and may be hard to fit for some applications [2].

Leaf springs are another commonly used concept of a decoupling mount design. It is a very simple flexible element – basically a single-strip flexure. Advantages of leaf springs include that their performance is easily controllable and that they are easily manufacturable while not increasing the dimensions of an optical system significantly. Spring dimensions can be selected by the ratio between tensile and bending stiffness so that it is flexible enough to bend under temperature fluctuations but remain stiff to endure launch loads. The analytical expression of these stiffnesses can be found in equations (2.1) and (2.2):

$$k_{tensile} = \frac{Eth}{l} \tag{2.1}$$

$$k_{bending} = \frac{Eth^3}{l^3} \tag{2.2}$$

Here k is the stiffness, E is the Young's Modulus of the leaf spring and l, t and h are the length, thickness and height, respectively [4]. Then the ratio between these is shown in equation (2.3):

$$\frac{k_{tensile}}{k_{bending}} = \frac{l^2}{h^2} \tag{2.3}$$

The third device isolating the system from mechanical and thermal environment is the so-called needles. It must be noted that they cannot be regarded as flexures since they are designed to remain stiff throughout the operational lifetime. In general, this mounting principle works on six separate elements each blocking one degree of freedom but leaving the other five unrestrained. For the first axis, three needles are added to support the system. Then, another two hold it at a right angle from the first axis. And on the last orthogonal axis, the sixth needle is fixed. This mount configuration can be seen in figure 2.2.

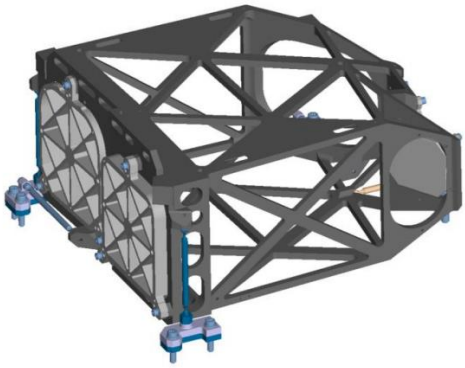

Figure 2.2 An overview of an optical instrument structure (grey) and interfaces (blue).

An advantage of the needle design is that it guarantees a minimal stress increase in the structure due to temperature fluctuations while adding to the instrument's dimensions only slightly. However, the vibrational isolation of such a system is poor since the needles do not provide any damping [5].

2.2 Thermal Control

Spacecraft thermal control is essential to guarantee that all of spacecraft systems operate optimally, i.e. in suitable thermal environment. Therefore, it is important to understand the factors that could influence the thermal balance reached on the satellite. Since space vacuum contains no particles that could transfer heat by convection, the main interactions for a spacecraft are the heat coming from the Sun or Earth, the heat radiated to deep space (radiation) and the heat flow between the satellite's hardware (conduction). System thermal balance can also be changed by selecting its materials according to their absorptance a and emittance ε ratio. For example, a satellite painted in

white will generally be cooler than one painted in black since white paint has a lower a/ε ratio than black.

The analytical solution for temperature balance is based on the conservation of energy and Stefan-Boltzmann laws. The emitted energy is equal to the one absorbed. This ratio can be found in equations (2.4) and (2.5):

$$Q_{out} = Q_{Sun} + Q_{planetary} + Q_{albedo} \tag{2.4}$$

$$\sigma \Delta T^4 \varepsilon A = q_S \alpha A + q_p \varepsilon A + q_a \alpha A \tag{2.5}$$

Here σ is the Stefan-Boltzmann constant, $\measuredangle T$ is the temperature difference between the balanced and ambient temperatures, q_S, q_p and q_a are the thermal radiation of the sun, planetary IR and planetary albedo, and a, ε and A are the coefficients of absorptivity and emissivity and area of a relevant surface. Then, the balance temperature can be determined from equation (2.6):

$$\Delta T = \sqrt[4]{\frac{q_S \alpha A + q_p \varepsilon A + q_a \alpha A}{\sigma \varepsilon A}} \tag{2.6}$$

As evident, the system's temperature greatly depends on the coefficients of absorptivity and emissivity which are highly variable for different materials and their finishes. Therefore, to reach the required operational temperature range, different arrangements of materials, finishes and paints should be examined to find the one that is optimal for the mission [6].

The coefficient of thermal expansion (CTE) is another relevant parameter for the project. It describes how the dimension of an object changes with temperature. Specifically, it measures the fractional change in size per degree of temperature. If the CTE is significantly different between the material of the mirror or lens and the rest of the support structure, e.g. aluminium, and the device operates in a thermally different environment than where it was assembled, additional stresses to the optical element may be introduced and the performance of an instrument may degrade. Other problems may arise when coating the mirrors. Mirror coatings can introduce surface distortions or even fracture over the operational temperature range if its CTE is dissimilar to the mirror's material. The only possible solutions are a CTE match which is often impractical and an isolation from the support structure via flexures [2]. Nonetheless, a CTE match can be achieved in a part of the system between adjacent elements. If, say, a primary and secondary mirror assembly is made from the same material, under temperature fluctuations all component and spacing dimensions will change equally. Such system is athermal because temperature changes do not affect focus or image quality and only small changes occur in the scale of the image [7].

2.3 Vibration

Since the flexure isolation acts not only against thermal fluctuations but also vibrations, it is important to know how they originate or build up as well. Resonance is one of the fundamental phenomena involving vibration. Resonance describes an increased vibration amplitude that occurs when the frequency of a periodically applied force is equal to a natural frequency of the system on

which it acts. This means that when a system is in resonance, a small force may excite a large response. This is especially relevant to a spacecraft during the launch phase of the mission when the rocket's engines may introduce such vibration that its hardware integrity could be compromised. The following equation (2.7) relates the member's approximate natural frequency f_N to its mass m and its structural stiffness k [7]:

$$f_N = \left(\frac{0.05}{\pi}\right)\left(\frac{k}{m}\right)^{1/2} \tag{2.7}$$

If the system's natural frequency is above the rocket's most intense vibrations during the launch, the danger of getting into resonance disappears. Therefore, as it can be seen from equation (2.7), a lower structure mass and a stiffer structure should be aimed for.

When analysing modal frequency simulation results, the modal mass participation factor becomes a thing to consider. This factor describes the percentage of the mass that is involved in a certain natural frequency mode. If the mass participation factor for a mode is low, it can generally be disregarded as the loads at that frequency do not have a large effect on the construction. On the other hand, if it reaches tens of percents, a catastrophic failure of a system can occur.

A space launch vehicle involves both sine and random vibrations. However, the latter are more dangerous since they typically show up at higher frequencies. Random vibrations are best quantified by the power spectral density (PSD). The PSD describes the strength of the energy as a function of frequency. Simply put, it shows at which frequencies the vibrations are strong and at which they are weak. To transform the energy numbers to a more conventional form, the root mean square (RMS) acceleration G_{RMS} response of a body vibrating randomly can be approximated to the multiples of gravity acceleration by the following expression (2.8):

$$G_{RMS} = \left(\frac{\pi f_N PSD}{4\eta}\right)^{1/2} \tag{2.8}$$

Here the PSD is defined at a frequency of the highest intensity, and η is a factor quantifying the effective damping of the system. Finally, since the most structural effects happen from the 3-sigma acceleration, the G_{RMS} value should be multiplied by 3 [7].

2.4 Optical Component Mounting

When integrating different telescope components into an assembly, the light beam obscuration should be minimized. Obscuration is a property of a telescope which quantifies the amount of light that passes through the optical system uninterrupted by an obstacle. It is defined in percent and the higher its value is, the better quality of the picture is achieved. This means that no parts of the telescope should obstruct the path of light towards the next optical component. That is, however, not always possible to accomplish. An easy way to check the telescope's obscuration is to draw a line through all the mirror and lens outer diameters and centres and see if any lines cross any hardware holding the mirrors or the rest of the structure.

For the reason that the project telescope could include some lenses in its configuration, several of their mounting options were reviewed. For this particular design, lens mounting should be simple, since space is limited, but also robust enough to ensure tight operating tolerances. Such lens retainers are snap rings, threaded rings or elastomeric retainers. The first of these is the simplest of all as it needs only a small groove located near a lens to snap-in. The only serious disadvantage of snap rings is that once in place, they are virtually impossible to take out. Threaded rings are relatively easy to machine as well. Such a system only needs an outer thread on the ring and an inner one on the lens tube. Threaded rings allow easy assembly and disassembly. This is also the most common method for precision mounting of lenses [8]. Elastomeric retainers are not as conventional or simple to integrate but they can work for the athermalization of an optical element. To do that, an elastomer ring needs a certain thickness to let the lens contract or expand freely in its tube. This thickness t_e may be determined by equation (2.9):

$$t_e = \left(\frac{D_G}{2}\right)\frac{(\alpha_M - \alpha_G)}{(\alpha_e - \alpha_M)} \tag{2.9}$$

Here a_G, a_M, a_e are the CTE's of the lens, mount, and elastomer, respectively, and D_G is the diameter of the lens [7]. Critical aspects of an elastomer for space application are low outgassing and resistance to a large temperature range.

Usually, tight tolerances of an optical system cannot be realized solely by precision manufacturing. Alignment shifts can occur due to, e.g., imperfections of a component machining process, temperature differences between the assembly and operational environment, applied loads or unevenly cured adhesive. For these reasons, optical alignment systems are used. There are several ways to tune a mirror or lens positioning. The most basic type of alignment mechanism is the push screws which essentially are threaded screws radially attached to the structure surrounding an optical element. They are simple to implement but a high precision can hardly be achieved. For a finer spacing adjustment, shims are used. Shims of certain thicknesses are inserted between a lens and a lens tube once the decentring value is estimated. This makes it possible to adjust the system precisely but any further corrections would be difficult to execute. With shims, tolerances of several microns are possible to achieve.

2.5 Design for Manufacturing

For the project, component manufacturing options are limited to lathing, milling and 3D printing. To optimize the costs, it is essential to know the pros, cons and limitations of each of these manufacturing methods. Lathing limits the production to rotationally symmetric parts only. However, it is more precise than most other manufacturing methods. Thus, when possible, telescope parts should be designed so that they are manufacturable by lathing. When milling, the size of the drill makes it unavailable to drill square edges. Internal geometries and deep undercuts cannot be machined either. Therefore, all the inner edges are rounded to the radius of the smallest available drill. The maximum undercut depth is recommended to be limited to 25 % of the hole radius where it is accessible. Finally, 3D printing offers great geometric flexibility and can produce custom parts quickly. But when tight tolerances or demanding structural properties are required, traditional manufacturing technologies are often a better option [9].

2.6 Industry Standards

To make the QKD CubeSat Telescope IOD mission achievable, it is necessary to take into consideration some of the industry standards. Without complying to these, even the best telescope design would not be allowed to be launched to space. Firstly, the European Cooperation for Space Standardization (ECSS) was created as an initiative to develop a coherent, single set of user-friendly standards for use in all European space activities [10]. The ECSS standards are not mandatory to follow by everyone as they are more of a recommendation than a requirement, however, many space agencies and companies have a strong commitment to support ECSS, thus, contractors also follow the standards. Moreover, since the mission in question will be launched on a CubeSat platform, the CubeSat Design Specification document mush be followed as well. In 1999, Cal Poly and Stanford University defined the necessary specification for the design, manufacture, and testing of a new type of small satellites intended for low Earth orbit (LEO). To this day, these requirements shall be followed to ensure a smooth launch and operation of a CubeSat. Lastly, as every rocket and, most importantly, its fairing structure have their own properties and dimensioning, the requirement document issued by the space launch provider must be respected too. This includes launch loads, its environment, payload volumetric constraints, etc.

3. Methods

3.1 SRR

One of the primary tasks of the project was to compile the SRR, or a system requirements review. This document evaluates the completeness of the instrument or system requirements necessary to fulfil the mission. To carry it out, all the given requirements and industry standards or even recommendations are put into a single table which helps to define the progress of completing the whole system. Given the tight industry's limitations, it may seem that the requirement list could be never-ending, however, since most of those were either non-applicable or were dismissed, it boiled down to a table of 25 criteria. Disregarded from the list were the requirements used only by the company's opticians, spacecraft standards that are not applicable to CubeSats or the telescope design in general, and some obvious engineering truths. After a successful completion of the SRR and the telescope's preliminary design, the results will be compared with design restrictions defined in the document.

A few separate requirement domains used to compile the SRR can be singled out:

1. ECSS
2. CubeSat Design Specification
3. Ariane 6 User's Manual
4. Customer

Since it is planned that the rocket launch service provider for the mission will be Arianespace, the user's manual for the company's future rocket was used. For the sake of simplicity, in the table only the name of the domain was identified as a reference and not its specific document number. The general requirement table from the SRR can be seen in table 3.1 below.

Table 3.1 General system's requirements.

ID	References	Criteria	Requirements	Comments
R1	ECSS	Gravity model	Alternative gravity models other than EIGEN-GLO4C may be used, provided that they are justified and validated.	The standard gravity value which is, by definition, 9.807 m/s^2 was used.
R2	ECSS	Solar energy flux	The values of 1321.6 W/m^2 for solar energy flux at aphelion and 1412.9 W/m^2 for solar energy flux at perihelion shall be used for electromagnetic radiation.	
R3	ECSS	Space sink temperature	A space sink temperature of 3 K shall be used.	
R4	ECSS	Earth albedo	For an orbiting spacecraft, the albedo values between 0.05 and 0.6 shall be used.	
R5	ECSS	Earth infrared	For an orbiting spacecraft, the Earth-emitted infrared radiation values of 150 W/m^2 to 350 W/m^2 shall be used.	
R6	Customer	Primary mirror diameter	The diameter of the primary mirror shall be 90 mm.	

R7	Customer	Exit beam diameter	The diameter of the exit beam shall be 3 mm.	
R8	Customer	Dimensions	The allowed envelope is 95 mm × 95 mm × 100 mm. The length may be relaxed slightly if required.	
R9	Customer	Exit pupil position	The exit pupil position shall be at least 20 mm from the rear 95 mm × 95 mm face of the telescope.	
R10	Customer	Mass	The telescope mass shall be less than 2 kg.	
R11	Customer	Thermal performance	The telescope shall be athermal between -10 °C and 40 °C.	
R12	Customer	Orbit	Assume polar or inclined LEO — 90 minute orbital period with 45 minutes in the Sun and 45 minutes in the shadow.	
R13	CubeSat Design Specification	Venting	The CubeSat shall be designed to accommodate ascent venting per ventable volume/area < 2000 inches (50 800 mm).	
R14	Recommendation [2]	Flexure positioning	To maintain optical alignment, flexure support forces should act through the CoG of the optical element.	
R15	Recommendation [1], [7], [11]	Resonance frequency	The resonance frequency should be higher than that of the driving forces by a factor of at least two.	Since the vibration intensity for the Ariane 6 launch vehicle drops off significantly at 700 Hz, the telescope's resonance frequency should be aimed to be at least 1400 Hz.
R16	Recommendation [12]	Mirror coating material selection	To reduce surface distortions over the operational temperature range, coating should have a similar CTE as the mirror.	
R17	Recommendation [4], [13]	Leaf springs	For athermalization and vibrational decoupling of small mirrors, leaf springs may be used.	
R18	Recommendation [14]	Temperature gradients	For a structural element, the temperature gradient should be less than 2 °C/mm and for an optical instrument, the temperature gradient should be less than 5 °C/mm.	
R19	Ariane 6 User's Manual	Qualification test factor	A safety factor of 1.25 shall be applied for static and sine vibration loads, a safety factor of 2 for random vibration load and a safety factor of 1.41 for shock load. For off-the-shelf payload adapters, a value of 10 % over the average static loads seen by the spacecraft shall be used.	
R20	ECSS, Ariane 6 User's Manual	Static loads	The system shall withstand an in-flight maximum static load for Ariane 6 launch vehicle which is -6 g axial and ±2 g lateral acceleration.	With the safety margin of 10 % and the safety factor of 1.25, the in-flight maximum static load for Ariane 6 launch vehicle is

				-8.25 g axial and ±2.75 g lateral acceleration.
R21	Ariane 6 User's Manual	Sine vibration load	The system shall withstand an in-flight maximum sine vibration load for Ariane 6 launch vehicle which is 1 g axial and 0.8 g lateral acceleration.	With the safety factor of 1.25, the in-flight maximum sine vibration load for Ariane 6 launch vehicle is 1.25 g axial and 1 g lateral acceleration.
R22	ECSS, Ariane 6 User's Manual	Random vibration load	For Gaussian distributed random loads for verification, the limit load contribution shall be derived as standard deviation multiplied by three, i.e. 3 × RMS. The RMS acceleration response shall be calculated at system's resonance frequency. The system shall withstand the random vibration load which is 0.04 g^2/Hz @ 150 - 700 Hz for Ariane launch vehicle.	With a conservative value of 5 % for the damping factor and the standard deviation multiplication, the RMS acceleration response according to equation (2.8) is 30.27 g for the metering structure and the secondary mirror system.
R23	Ariane 6 User's Manual	Shock load	The system shall withstand an in-flight maximum shock load for Ariane 6 launch vehicle which is 1000 g in -Z direction.	With the safety factor of 1.41, the in-flight maximum shock load for Ariane 6 launch vehicle is 1410 g in -Z direction.
R24	ECSS, CubeSat Design Specification	Material selection	CubeSat materials shall satisfy the following low out-gassing criterion to prevent contamination of other spacecraft during integration, testing, and launch: 1. CubeSats materials shall have a Total Mass Loss (TML) < 1.0 %. 2. CubeSat materials shall have a Collected Volatile Condensable Material (CVCM) < 0.1 %.	
R25	ECSS	Material design allowable	All design allowables for metals, non-metals and composite materials (stress or strain) shall be defined by their mechanical property values above which at least 99 % of the population of values is expected to fall, with a confidence level of 95 % (A-values). All design allowables for adhesive materials in bonded joints (stress or strain) shall be defined according to standards agreed with the customer. For metallic and alloy, the elastic modulus may be based on values certified by the manufacturer.	Yield strength used: Aluminium 7075 – 500 MPa; Invar 36 – 483 MPa. CTEs used: Aluminium 7075 – $2.34 \cdot 10^{-5}$ m/(mK); Invar 36 – $1.30 \cdot 10^{-6}$ m/(mK).

In the original SRR document that was prepared for the company, the verification and test requirements were included. As these would later double in the test plan section of the results chapter, they were omitted here.

3.2 Trade Studies

Two trade studies had to be performed to evaluate several design concepts against each other and the previously defined requirements. They were carried out for the semi-kinematic mounting design and the secondary mirror mount design.

The first of the studies included the following design options:

1. Leaf springs
2. Needles
3. Bipods
4. Elastomeric mounting

The leaf spring option offers good athermalization, not the best but acceptable vibrational decoupling and low design complexity and bulkiness which becomes important when having tight dimensional constraints [4]. The needle design concept was not satisfactory for the project since it is good for athermalization but not for vibrational decoupling. Both bipod structure and elastomeric mountings are good for isolation, however, bipod structure would add complexity to the design and would not be suitable for a very limited volume of the system while elastomeric mountings not only would inevitably increase the lateral dimensions of the system (equation (2.9)) but would also introduce larger alignment errors when adhesive cures [5], [7]. Therefore, leaf springs were the best semi-kinematic mounting design option for the project since their performance is controllable and they are easily designed while not increasing the dimensions of the telescope significantly. Leaf springs also provide limited shock and vibration resistance. The leaf spring flexure design is displayed in figure 3.1.

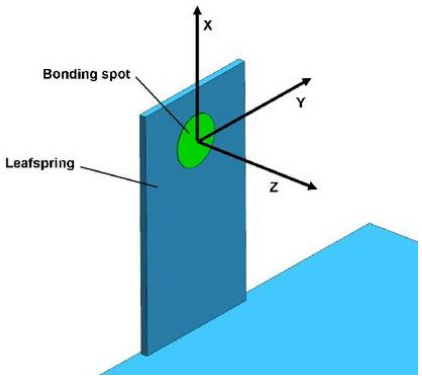

Figure 3.1 Leaf spring concept.

Table 3.2 gives the conclusion of the semi-kinematic mounting design trade study between the four mentioned concepts.

Table 3.2 Semi-kinematic mounting design trade study.

	Leaf springs	**Needles**	**Bipods**	**Elastomeric mounting**
Athermalization	GOOD	GOOD	GOOD	GOOD
Vibrational decoupling	ACCEPTABLE	POOR	ACCEPTABLE	GOOD
Complexity	LOW	MODERATE	HIGH	MODERATE
Bulkiness	LOW	LOW	HIGH	MODERATE

The secondary mirror mount design trade study included the following options:

1. Centred tripod
2. Tripod
3. Box structure + spider

When selecting the secondary mirror mounting, or a metering structure, it was already known that the telescope system shall be encased in a rectangular box structure to further isolate it from the environmental changes. Therefore, a more typical configuration of a cylinder and spider mounting had to be dismissed. Perhaps the most prominent criterion in the trade study was if the thermal and vibrational decoupling for the structure is required to be designed again. If the leaf springs would already decouple the system from these factors, the need for another isolating system could be avoided if the structure was attached to the primary mirror. From the studied options, only a centred tripod configuration would allow that. Therefore, its complexity was evaluated as the lowest of all designs. The box structure + spider concept would have the highest resonance frequency since its structure bars would be the shortest which also translates to highest stiffness. None of the designs would avoid beam path obscuration on the mirrors and for this criterion all the options would perform equally. However, the need of separate decoupling system on the spider arms outweighs its good resonance properties. Thus, the centred tripod configuration was concluded as the best. An example of its design can be seen in figure 3.2.

Figure 3.2 AOS's AP Series Satellite Telescope's centred tripod configuration.

The tripod consists of three structural bars connecting the secondary mirror and the base that is fixed to the primary mirror. To raise the resonance frequency of the system, the metering structure should be made as stiff as possible while not increasing its mass too much near the top. Thus, the bars should be made thicker and a cylinder shall connect all of those at the base. However, the metering structure's stiffness usually conflicts with the obscuration of the telescope and a balance has to be reached.

Table 3.3 shows the conclusions for the second trade study.

Table 3.3 Secondary mirror mount design trade study.

	Centered tripod	**Tripod**	**Box structure + spider**
Resonance frequency	MODERATE	LOW	HIGH
Obscuration	MODERATE	MODERATE	MODERATE
Complexity	LOW	MODERATE	HIGH
Resonance frequency	MODERATE	LOW	HIGH

3.3 FEA Simulations

Design validation was done by FEA when running Autodesk Fusion 360 simulation studies. To get accurate results, it was crucial to set each of them up properly. Several kinds of simulations were performed:

1. Static stress
2. Modal frequencies
3. Thermal
4. Thermal stress
5. Mirror coating thermal stress

When running the static stress simulation, the minimum factor of safety in the structure under a shock load was indicated. The modal frequency analysis helped identify the natural frequency modes of the optical payload. Thermal simulations were set to check for the highest temperature gradients. Thermal stress studies showed safety factors and misalignments of the optical elements under different ambient temperatures. Finally, the mirror coating thermal stress simulation allowed to check if the mirror coating cracked under temperature fluctuations by calculating the stresses in materials.

The system's coordinate frame was used to better describe the simulation study setups. It is displayed in figure 3.3.

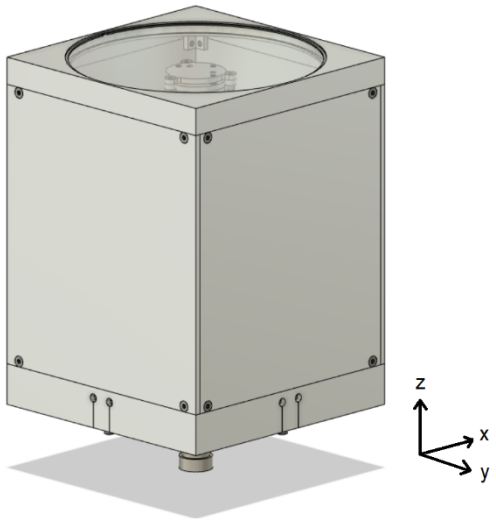

Figure 3.3 QKD CubeSat telescope with its coordinate frame.

3.3.1 Static Stress Simulation

While the maximum static load for Ariane 6 launch vehicle is -8.25 g axial and ±2.75 g lateral acceleration, and the RMS acceleration response from random vibration is 30.27 g for the secondary mirror system, highest stresses are reached from the shock load which is 1410 g. Thus, a gravity acceleration was set to $1410 \cdot 9.807 \approx 13800$ m/s^2 and applied in the -Z direction.

To make the telescope system constrained and ready for the simulation, it was fixed at 4 mounting points at the box structure base and optical table interface which can be found on the -Z face of the telescope.

3.3.2 Modal Frequencies Simulation

Similar to the static stress simulation, the telescope system had to be fixed at four mounting points at the box structure base and optical table interface.

When analysing the modal frequencies simulation results, the modal mass participation factor table was enabled. As Autodesk Fusion 360 also shows resonance frequency modes that involve only a tiny fraction of the system's mass, some of those can be disregarded. Therefore, the mass participation factor limit of 5 % was set for the simulation results that were further investigated.

3.3.3 Thermal Simulation

For both thermal and thermal stress simulations, certain solar energy flux, Earth albedo and Earth infrared radiation values were used for the hot and cold cases of simulations. Naturally, the upper bound values defined in the SRR requirement table were used for the hot cases and the lower bound values for the cold cases.

Hot case

Two heat sources originating from two opposite directions were applied. From +X, +Y side, the solar energy flux value of 1412.9 W/m^2 or $1412.9 \cdot \sin(45°) \approx 999$ W/m^2 since the heat can only be applied at the right angle was set. From -X, -Y direction, the planetary energy flux value of $1412.9 \cdot 0.6 + 350 \approx 1198$ W/m^2 or $1198 \cdot \sin(45°) \approx 847$ W/m^2 was applied. From -Z side, the internal satellite temperature of 40 °C was applied at points where the box structure base interferes with the optical table. This simulation setup can be seen in figure 3.4.

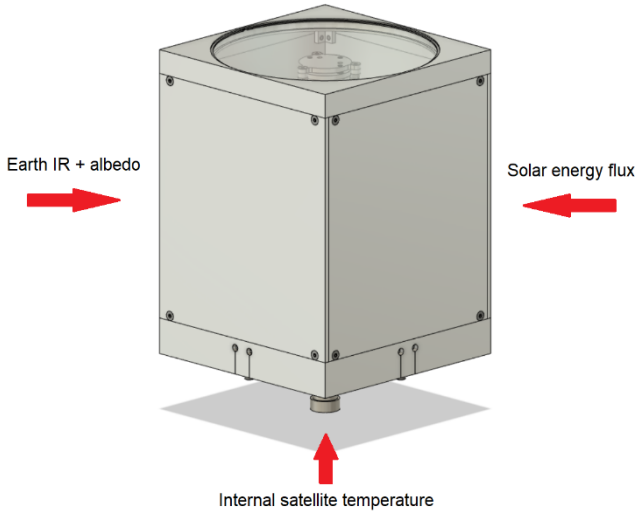

Figure 3.4 Hot case of the thermal simulation setup.

On all telescope system faces except for the ones where the internal satellite temperature was applied, an a/ε ratio of 0.7 for aluminium and 0.5 for glass with an ambient temperature of 3 K was applied. Finally, the global initial temperature of 20 °C was set.

Cold case

Since the cold case happens at a time of eclipse, only the planetary IR value of 150 W/m^2 from +X side was applied. From -Z side, the internal satellite temperature of -10 °C was applied. This simulation setup can be seen in figure 3.5.

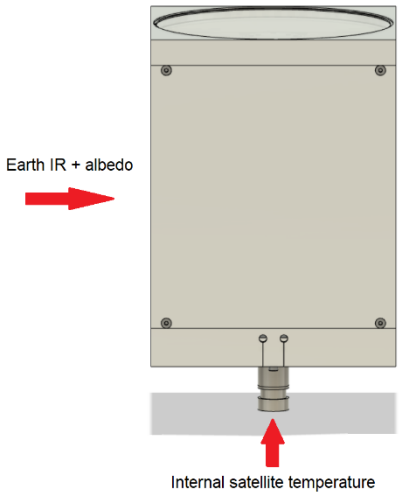

Figure 3.5 Cold case of the thermal simulation setup.

All radiation and global initial temperature conditions were applied the same way as for the hot case.

3.3.4 Thermal Stress Simulation

Hot case

The temperature of 40 °C was applied to all faces of the telescope system. Since the rest of the satellite has the same temperature, frictionless constraints were set for the box structure base and optical table interface. The default stress-free temperature was set to 20 °C.

Cold case

The temperature of -10 °C was applied to all faces of the telescope system. Frictionless constraints were set for the box structure base and optical table interface. The stress-free temperature was set to 20 °C.

Asymmetrical heating case

To check for the largest decentring in the telescope system, two heat sources with the largest energy difference between each other were applied from two opposite sides. From +X, +Y side, the solar energy flux value of 1412.9 W/m^2 or $1412.9 \cdot \sin(45°) \approx 999$ W/m^2 was applied. From -X, -Y direction, the planetary energy flux value of $1412.9 \cdot 0.05 + 150 \approx 221$ W/m^2 or $221 \cdot \sin(45°) \approx 156$ W/m^2 is applied. From -Z side, the internal satellite temperature of -10 °C is applied at points where the box structure base may interfere with the optical table. This simulation setup is similar to the thermal simulation hot case and can be seen in figure 3.5.

On all telescope system faces except for the ones where the internal satellite temperature was applied, an a/ε ratio of 0.7 for aluminium and 0.5 for glass with an ambient temperature of 3 K was applied. Finally, the stress-free temperature was set to 20 °C.

3.3.5 Mirror Coating Thermal Stress Simulation

To check the possibility of cracks appearing in the mirror coating layers due to temperature fluctuations, a thermal stress test was run for both primary and secondary mirrors. Since the use of potential coating materials is classified, in this report the mirror coating materials will be material A on the mirror and a layer of material B on top of material A.

To save computational time and increase the meshing density of the mirror, only a quarter of the mirror was modelled for both the primary and secondary mirror.

For both mirror simulations, the operating temperature extremes of -10 °C and 40 °C were applied to all faces of mirrors. To imitate the full mirror model, frictionless constraints were set for the inside walls and the base of the mirror. The stress-free temperature was set to 20 °C for all studies.

4. Results

4.1 System Components

The preliminary design of the QKD CubeSat telescope will be comprised of these components: primary mirror (M1), secondary mirror (M2), M2 structure, metering structure, lens tube 1 (LT1), paraxial lens 1 (PL1), lens tube 2 (LT2), paraxial lens 2 (PL2), two threaded rings, lock ring, box structure base, four box structure panels, box structure top, sun window, snap ring, 19 × M2 316 stainless steel hex drive flat head screws, 6 × M1.6 316 stainless steel socket head screws and 4 × M2 316 stainless steel socket head screws.

How these will be integrated into the telescope assembly is shown in figures 4.1 and 4.2. It should also be noted that only the visible components are identified in the images as the looks of the insides of the optical payload are classified.

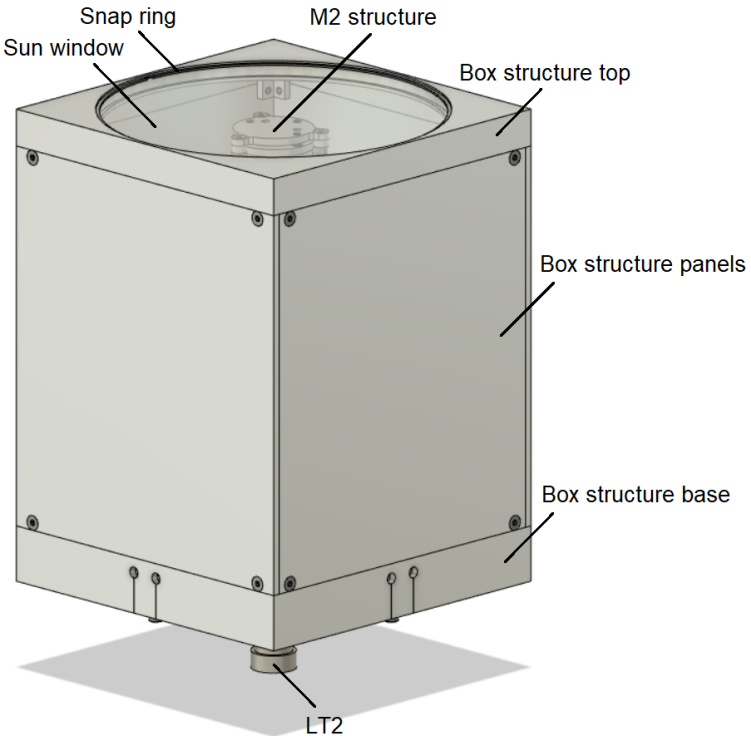

Figure 4.1 Top-front view of the QKD CubeSat telescope.

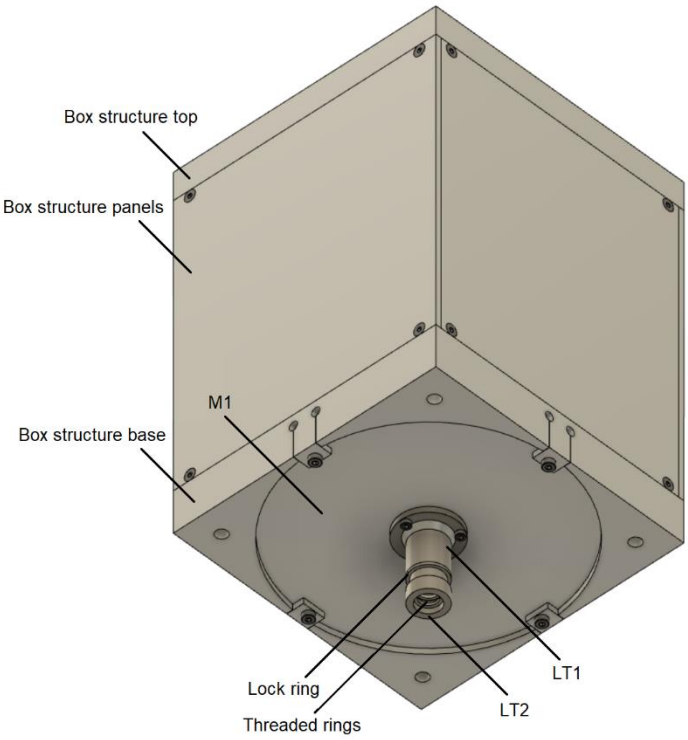

Figure 4.2 Bottom-front view of the QKD CubeSat telescope.

4.2 Materials

All telescope components except for the sun window, lenses, lens tubes and fasteners were designed to be manufactured from aluminium 7075 alloy. PL1 and PL2 will be made of glasses BK7G18 and SF6G05, respectively. Lens tubes and the lock ring between them will be manufactured from invar 36.

4.3 Assembly

The M1 will be thermally and vibrationally isolated from the box structure base with four leaf springs which are visible in figure 4.2. Then, the metering structure with the M2 at its end will be mounted to the +Z side of the M1, and the LT1 will be attached to the -Z side of the M1. The PL1 and PL2 will be fastened to the lens tubes with two threaded rings. When the sun window is locked to the box structure top with the snap ring, the whole box structure with its four panels will be assembled to the box structure base. Finally, the box structure base will be mounted to the rest of the satellite on the optical table which is located in the -Z direction from M1.

4.4 Optical Alignment

During the optical system alignment, back optics (lens tubes with the paraxial lenses) will be calibrated first. Focus corrections in the axial direction will be made by moving the lens tubes with respect to each other in a thread and then securing them in place with the lock ring. Lateral corrections to fix decentring will be made by inserting shims in between the paraxial lenses and the lens tube walls. When the back optics are attached to the M1, the rest of the system will be

calibrated using the 3-axis kinematic mount of the M2. These alignment mechanisms are further described in the next report section.

4.5 Component Design

4.5.1 Primary Mirror

The primary mirror M1 will be mounted to the box structure with four leaf springs that make the telescope thermally and vibrationally decoupled. To isolate additional mounting stresses from the mirror surface, an undercut above the leaf spring bonding points will be machined in the mirror. A similar undercut will separate LT1 from M1 as it will be manufactured from a different material than M1 and additional stresses will be introduced at the mounting points due to different CTE's. An example of this optical component mounting principle is displayed in figure 4.3. To remove the need of additional thermal and vibrational isolation, all other QKD telescope components will be mounted on M1.

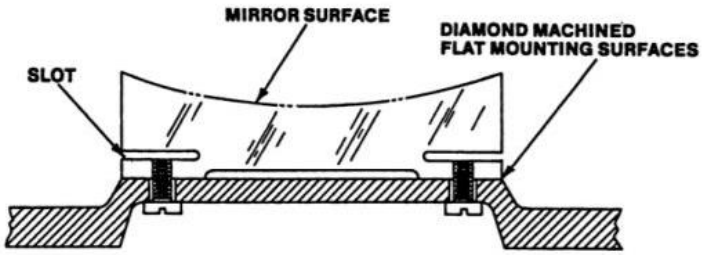

Figure 4.3 Stress-free mounting for a small metal mirror with undercuts.

4.5.2 Secondary Mirror

To enable the secondary mirror alignment adjustment option for the telescope, M2 will be attached to a 3-axis kinematic mount structure which will allow to change mirror's tip, tilt and focus. Two M2 structure plates will be connected with two springs inserted between three grub screws that will adjust the second plate's alignment. M2 will be fixed to the plate with epoxy adhesive. The kinematic mount design was based on Thorlabs' K5X1 mount which is shown in figure 4.4.

Figure 4.4 Thorlabs K5X1 5-Axis Kinematic Mount.

4.5.3 Metering Structure

The centred tripod configuration was chosen for the metering structure design. Its example can be seen in figure 3.2. Both a cylinder at the base and thicker bars were incorporated into the design to raise the structure's resonance frequency.

To check if the metering structure blocks any incoming light, a light beam path was drawn all the way from the rays coming through the sun window to the back optics' exit pupil. Throughout the whole optical payload, only a small fraction of light was absorbed by hitting the sides of the metering structure bars.

4.5.4 Lens Tubes

For focus corrections, lens tubes were designed to be adjustable along the optical axis. It will be done with a system of two threaded lens tubes and a lock ring that secures the mechanism in wanted position. PL1 and PL2 will be fixed in place by threaded rings. The mechanism design was based on Thorlabs' SM05V05 lens tube which is shown in figure 4.5.

Figure 4.5 Thorlabs SM05V05 Adjustable Lens Tube.

4.5.5 Box Structure

The box structure was designed to offer higher flexibility in terms of integration to the satellite platform and better protection from temperature fluctuations during the operational stage of the telescope. To facilitate box structure's machinability, it will be assembled from six parts – its base, top and four panels on the sides.

Designed at the box structure base, four leaf springs are the main isolating interface of the optical payload. Their dimensions were selected according to equation (2.3) so that they are flexible enough to bend under temperature fluctuations but remain stiff to endure launch loads. To reduce stress concentrations at the ends of the leaf spring slits, rounded cuts were made at these points. These also act as venting holes which ensure that during the launch phase the pressure difference inside the box and outside of it does not build up. A detailed view of the leaf spring is shown in figure 4.6.

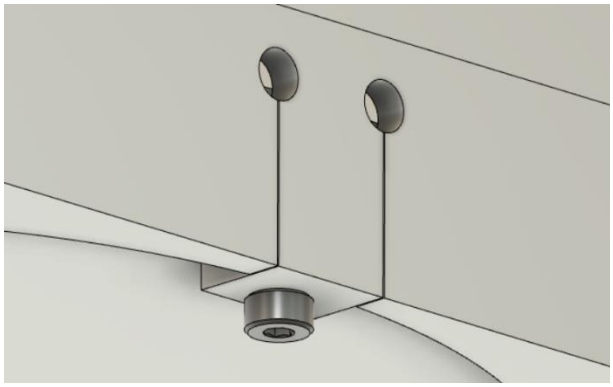

Figure 4.6 Leaf spring of the QKD CubeSat telescope.

4.6 FEA Simulations

4.6.1 Static Stress Simulation

The minimum safety factor was 1.24 and was the lowest at the box structure & optical table interface points.

4.6.2 Modal Frequencies Simulation

The first mode of the resonance frequency was at 162 Hz but applied only to the secondary mirror structure or to around 1 % of the mass of the system. The mass participation factor was larger at 1338 Hz for 26 % of the system's mass.

As the vibration intensity for the Ariane 6 launch vehicle drops off significantly at 700 Hz, according to modal frequency analysis, the optical payload resonance frequency was higher than that of the driving forces by a factor of 1.91.

4.6.3 Thermal Simulation

Hot case

The maximum temperature gradient was 1.52 °C/mm for a structural element and 2.10 °C/mm for an optical instrument.

Cold case

The maximum temperature gradient was 0.83 °C/mm for a structural element and 1.16 °C/mm for an optical instrument.

4.6.4 Thermal Stress Simulation

Hot case

Even though the maximum stresses were below the safety factor of 1 and were equal to 0.75 at the edge of the PL2, when inspected more carefully it could be seen that the stresses were very

concentrated at one point of the PL2 and were an artefact of finite element analysis approximations and meshing. This stress concentration can be seen in figure 4.7.

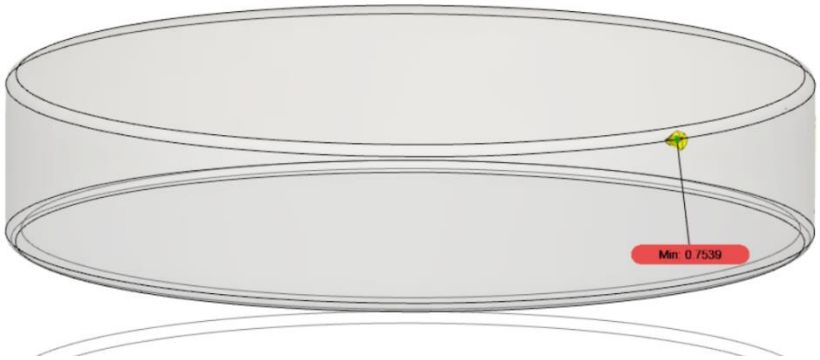

Figure 4.7 Thermal stress hot case simulation for the PL2.

The absolute displacement between the two mirror centre points in Z axis was 50.9 μm.

Cold case

The minimum safety factor was 1.05 and was the lowest at the sun window mounting points.

The absolute displacement between the two mirror centre points in Z axis was 76.3 μm.

Asymmetrical heating case

The primary mirror decentring in Y axis was 0.99 μm. For the same study, the secondary mirror decentring was 0.64 μm.

4.6.5 Mirror Coating Thermal Stress Simulation

Primary mirror

For the operating temperature of -10 °C, the maximum stress in material B amounted to 25 % of yield limit and in material A from 50 % to 173 % of the yield limit, depending on the chosen material A type. For the operating temperature of 40 °C, the maximum stress in material B amounted to 36 % of yield limit and from 34 % to 118 % in material A.

Secondary mirror

For the operating temperature of -10 °C, the maximum stress in material B amounted to 26 % of yield limit and in material A from 65 % to 223 % of the yield limit. For the operating temperature of 40 °C, the maximum stress in material B amounted to 31 % of yield limit and from 55 % to 191 % in material A.

4.7 Test Plan

As the QKD CubeSat telescope is still under development, the test plan may change in the future. However, at the moment of writing the thesis report, the optical alignment, the gravity release, the launch load (sine vibration and shock load) and the thermal vacuum qualification tests are planned.

Visual inspection, mass measurement and interface verification, as well as modal survey and random vibration tests, may also be performed.

For these tests, the accuracies of measurements were identified in the SRR:

1. Mass: ±0.05 % or 1 g whatever is the heavier;
2. CoG: within a 1 mm radius sphere;
3. Moment of inertia: analysis of the detailed CAD model to an accuracy of ±5 %;
4. Temperature: by case;
5. Acceleration and static load: ±10 %;
6. Frequency for mechanical tests: ±2 % (or ±1 Hz whichever is greater);
7. Strain: ±10 %.

4.7.1 Optical Alignment Test

Dimensional stability tests will be performed on optical telescope hardware to verify that the optics fulfil the mission performance requirements under all expected operational conditions. The optical alignment calibration under a natural gravity load will be done for the telescope system mirrors and lenses to reach the optimal modulation transfer function.

The optical alignment approach was described in more detail in the optical alignment section of this chapter.

4.7.2 Gravity Release Test

The gravity release test has the main objective to assess the effects of the absence of gravity loads for the on-orbit configuration being in contrast with the measurement conditions on Earth. On such test, the potential defocus or decentring of an optical instrument can be quantified which occurs in space by the release of the gravity loads.

During the test only two setup directions will be considered: axial and lateral, and therefore two loading directions will be tested. The test specimen will be constrained at its mounting interfaces. For the test, the unloaded state will conform to the natural gravity acting on the test specimen. Gravity compensation loads will then be applied to the unloaded state and the deformations will be measured.

4.7.3 Launch Loads Test

Sine vibration

Sinusoidal tests will be conducted in the launch configurations on each of 3 orthogonal axes. A resonance search will be performed before and after the sinusoidal vibration test to determine resonance frequencies to evaluate the space segment equipment integrity.

The success criteria for the resonance search will be:

1. Less than 5 % in frequency shift, for modes with an effective mass greater than 10 %;
2. Less than 20 % in amplitude shift, for modes with an effective mass greater than 10 %.

For the test, a sinusoidal sweep at 2 oct/min for the 5 Hz - 140 Hz range will be performed.

Shock load

The shock tests demonstrate the ability of the space segment equipment to withstand the shocks encountered during the spacecraft separation. The equipment will be mounted to a fixture using its normal mounting points. The selected test method will achieve the shock response spectrum with a representative transient, comparable in shape and duration to the expected in-flight shock. For the Ariane 6 launch vehicle it is presented in figure 4.8. Hardware integrity will be verified after the test.

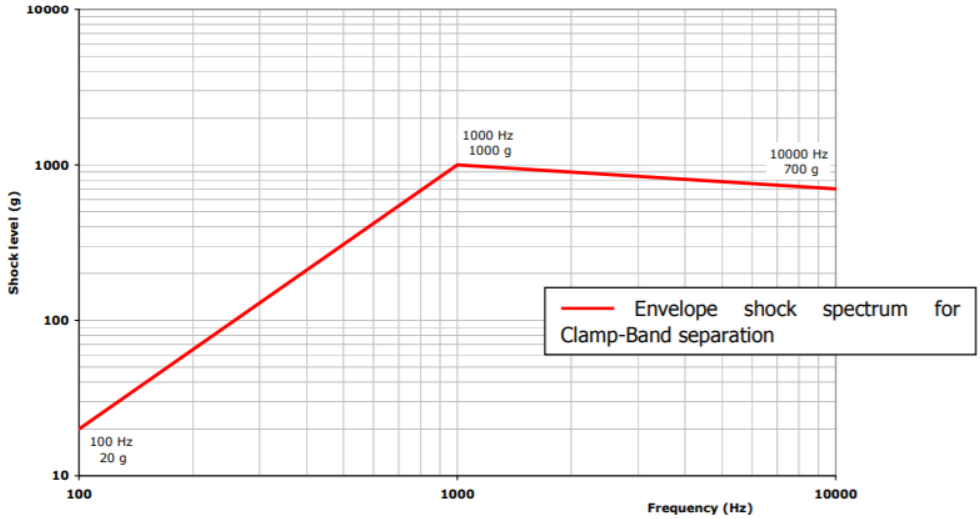

Figure 4.8 Ariane 6 shock response spectrum for the spacecraft separation phase.

The applied shock load level will be equal to the maximum expected shock spectrum +3 dB qualification margin. The shock duration will be 20ms.

4.7.4 Thermal Vacuum Test

Thermal vacuum test is performed for space segment equipment whose operation occurs in space vacuum environment at any time of its lifetime. The test is performed at a pressure of 10^{-5} hPa or less.

The test profile should start with a maximum non-operating temperature. The test will be performed by completing 8 thermal cycles of temperatures swinging from maximum to minimum non-operational temperature with a qualification margin of ±5 °C.

5. Discussion

Since the design process mostly revolved around the relationship between the SRR requirements and the FEA analysis results, it would be reasonable to start the discussion chapter by running through all the studies executed in Autodesk Fusion 360 software.

Firstly, the static stress simulation results were satisfactory. The minimum safety factor was 1.24. It already included the safety margin defined in requirement R19 of the SRR which means that any number above 1 given for the study result would be sufficient. Also, the random vibration load described in R22 could become higher as the damping factor is hard to define without doing any testing on hardware, but it is very unlikely it would be as damaging to the structure as the shock load which the static stress study was based on. Of course, different from the shock load, the random vibration could work on the telescope in a lateral direction, however after running a few quick simulations with such setup, it was clear that the structure would remain robust.

Both the modal frequency and thermal studies were satisfactory as well. Even though the results of the former study did not quite reach the recommended value of the resonance frequency to the driving forces frequency ratio of two that is defined in R15, it is safe to assume that after some improvements to the telescope this ratio will be reached. Whereas, when comparing the thermal simulation outcomes to requirement R18, it can be seen that the results never exceeded the recommended values of a temperature gradient of 2 °C/mm for a structural element and 5 °C/mm for an optical instrument.

The thermal stress studies were trickier to analyse since they were more susceptible to the way they were set up and their calculations were the lengthiest. Stress concentrations appearing at seemingly random points were possible to get rid of only by increasing the mesh density, but such studies took a few hours to run and were impractical to reiterate if the results were still inconclusive. Therefore, the result of the hot case was left at the safety margin of 0.75 with a hope that further testing would show the back optics' actual performance. As for the displacement and decentring values, they were on the same order of magnitude as the expected performance from the mBryonics' opticians, however the exact limitations were still not defined at the time of the submission of this report. To calculate these values and to make sure the design satisfies them will be one of the main tasks for the future of the QKD CubeSat telescope project.

The last Autodesk Fusion 360 simulation, the mirror coating feasibility study, revealed that certain materials are possible to be used for the coating only if the tougher form of material A could be acquired. It was assured that it would not be a problem by the colleagues.

Aluminium 5005, 5052, 6061, 7075, invar 36 and beryllium were considered when choosing the material for the rest of the telescope. Out of all aluminium alloys, 7075 was chosen due to its highest strength which allowed to reduce the structure's mass while maintaining the same performance. Invar was chosen for the lens tubes due to its very low CTE which better matched the CTE of glass paraxial lenses and, thus, reduced thermally induced stresses. Beryllium was dismissed for its high toxicity and cost. All aluminium alloys considered are used for both the main CubeSat structure and the rails. When all optical and mechanical components are made from the same material, shift from the fabrication and assembly temperature on Earth to the cryogenic temperature in space will change all component dimensions equally, thus only the scaling of the images will be affected. Therefore, it was convenient to use the same material for box structure and to further minimize thermally induced stresses.

Additionally, the preliminary QKD CubeSat telescope design was estimated to weight around 518 g which is well below the allowable mass of 2 kg defined in R10. Even then it is expected to be further reduced by doing mass optimization for the telescope's detailed design version. At the moment of the report submission, all the box structure side panels were designed to be metal sheets of the same thickness. This may be changed by executing additional FEA simulation iterations and by cutting out some of the material when forming a perforated pattern on the panels. Moreover, at the current stage of the project, lightweighted design of both mirrors was not considered. However, many processes creating structural patterns at the back side of the mirror exist which generally form a honeycomb-like configuration.

Furthermore, during the telescope's design detailing phase, thermal control will be another important task to work on. For the thesis project, only the temperature gradients and thermally induced stresses were analysed. When changing the material finishing, these gradients and stresses could be reduced more. As seen in equation (2.6), the temperature balance can mostly be changed by modifying the a/ε ratio of materials, i.e. their finish. For example, the box structure could be brushed, polished or even painted, depending on if the stresses are largest at a cold or hot case of operation. Payload's thermal properties will be improved by adding insulation at certain parts of the optical system as well. This will further isolate the telescope from temperature fluctuations in the satellite.

Finally, when the QKD CubeSat telescope's mass is optimized and the means of thermal control are managed, its preliminary prototyping and testing will be commenced. The mechanical design of the optical payload relied heavily on FEA. Analysis allowed to understand things like the stresses expected in the components, how to mitigate them, the structural dynamics in different thermal and vibrational environments. FEA also gave the first prediction of these metrics. With this knowledge and a detailed enough design of the telescope, prototype hardware will be machined, assembled and tested to validate the finite element model. Early testing will help to win time for the improved design decisions and even additional testing without having a major impact on the project's schedule. Prototyping and testing will lead on the non-linear and time domain FEA which was beyond the scope of the preliminary design phase of the project. This will be one of the final iterations of the optical payload designs after which the assembly, integration and test (AIT) plan will be composed. The AIT plan will be the benchmark of a proper end product preparation for the launch and the completion of the mission.

6. Conclusions

Over the time of working on the QKD CubeSat telescope project, the challenge of making the FSO technology affordable got a little closer to realization. Together with the mBryonics team, the prototype of the optical payload mounting interface for the QKD CubeSat telescope IOD was designed. Along the way, a thorough literature study involving each telescope component was performed, the SRR was compiled and numerous FEA simulations were run.

One of the main problems met while designing an optical system for space application was to maintain the component alignment to the highest precision in harsh operating conditions. It was overcome – the optical distortions should be kept to a minimum with mirror displacement and decentring values never exceeding tens of microns. As the exact limitations for these are not set yet, the dimensional stability aspect may be worked on further in the future. It was made possible by mounting the optical payload on leaf spring flexures which isolate the rest of the structure from temperature changes and vibrations produced by rocket engines during the space launch. Not only that – leaf springs were designed to be robust enough to hold the telescope during a potential shock load of 1000 g and at the same time offer flexibility to maintain their athermalization properties. Finally, the optical system design ensures that the most intense random vibrations induced during the rocket launch will not damage the system as its resonance frequency is almost two times higher than that. The structure's performance should be checked in practice at a later stage of the project following the test plan which was also prepared during the thesis work period.

Although an optional objective of 3D printing, assembling and testing the structure to validate its FEA results was raised initially, it was not fulfilled as the current global epidemiological situation forced to produce most of the thesis project remotely and the finish of it was delayed by a few weeks. Nevertheless, the work will continue shortly at the office. Firstly, the future tasks reviewed in the previous chapter will be focused on. Then, hopefully, the design will be brought to full fruition and the QKD CubeSat telescope will be flung to space in 2022.

Bibliography

[1] Weatherwax, M.S. and Doyle, K.B. (2014). Vibration Analysis and Testing for the LLST Optical Module. *Current Developments in Lens Design and Optical Engineering*, XV.

[2] Vukobratovich, D. and Richard, R.M. (1988). Flexure mounts for high-resolution optical elements. *Optomechanical and Electro-Optical Design of Industrial Systems.*

[3] Kihm, H., Yang, H.S., Moon, I.K., Yeon, J.H., Lee, S.H. and Lee, Y.W. (2012). Adjustable bipod flexures for mounting mirrors in a space telescope. *Applied Optics*, 51(32), 7776.

[4] Te Voert, M.J.A., Vosteen, A., Mekking, J., Nijland, B. A., Pijnenburg, J., de Vreugd, J. and van Werkhoven, W. (2012). Ultra stable iso-static bonded optical mount design for harsh environments. In E. Armandillo, N. Karafolas and B. Cugny (Eds.), *International Conference on Space Optics — ICSO 2012*.

[5] Freudling, M., Klammer, J., Lousberg, G., Schumacher, J.M. and Körner, C. (2016). New isostatic mounting concept for a space born Three Mirror Anastigmat (TMA) on the Meteosat Third Generation Infrared Sounder Instrument (MTG-IRS). In R. Navarro and J.H. Burge (Eds.), *Advances in Optical and Mechanical Technologies for Telescopes and Instrumentation II*.

[6] Jacques, L. (2013). *Spacecraft Thermal Control.* [online] Available at: http://www.ltasvis.ulg.ac.be/cmsms/uploads/File/2013_11_04_Satellite_Engineering_THER_LJ(2).pdf

[7] Yoder, P.R. (2008). *Mounting optics in optical instruments*. Bellingham, Wash.

[8] Burge, J. (2011). *Mounting of Optical Components. Mounting of lenses.* [online] Available at: https://wp.optics.arizona.edu/optomech/wp-content/uploads/sites/53/2016/08/26-Mounting-of-lenses-1.pdf

[9] Redwood, B., Schöffer, F. and Garret, B. (2018). *The 3D printing handbook: technologies, design and applications*. Amsterdam, The Netherlands: 3D Hubs B.V.

[10] ECSS. (2020). *Standards | European Cooperation for Space Standardization*. [online] Available at: https://ecss.nl/standards/

[11] Steele, J.M., Vallimont, J.F., Rice, B.S. and Gonska, G.J. (1992). A compliant optical mount design. In D.M. Aikens, V.L. Genberg, G.C. Krumweide and M.J. Thomas (Eds.), *Design of Optical Instruments.*

[12] Nevin, K.E., Doyle, K.B. and Pillsbury, A.D. (2011). Optomechanical design and analysis for the LLCD space terminal telescope. In M.A. Kahan (Ed.), *Optical Modeling and Performance Predictions*, V.

[13] Kihm, H., Yang, H.S. and Lee, Y.W. (2014). Bipod flexure for 1-m primary mirror system. *Review of Scientific Instruments*, 85(12), 125101.

[14] Poinas, P. (2004). *Satellite Thermal Control Engineering.* [online] Available at: http://www.tak2000.com/data/Satellite_TC.pdf

TRITA-SCI-GRU 2020:295